Eur. Phys. J. C 26, 345–355 (2003)
Digital Object Identifier (DOI) 10.1140/epjc/s2002-01071-8

THE EUROPEAN PHYSICAL JOURNAL C

Measurement of the $b\bar{b}$ production cross section in 920 GeV fixed-target proton-nucleus collisions

The HERA – B Collaboration

I. Abt[28], A. Abyzov[26], M. Adams[11], H. Albrecht[13], V. Amaral[8], A. Amorim[8], S. J. Aplin[13], A. Arefiev[25], I. Ariño[2], M. Atiya[36], V. Aushev[18], Y. Bagaturia[13,43], R. Baghshetsyan[13,44], V. Balagura[25], M. Bargiotti[6], S. Barsuk[25], O. Barsukova[26], V. Bassetti[12], J. Bastos[8], C. Bauer[15], Th. S. Bauer[32,33], M. Beck[30], A. Belkov[26], Ar. Belkov[26], I. Belotelov[26], I. Belyaev[25], K. Berkhan[34], A. Bertin[6], B. Bobchenko[25], M. Böcker[11], A. Bogatyrev[25], G. Bohm[34], C. Borgmeier[5], M. Bräuer[15], D. Broemmelsiek[12], M. Bruinsma[32,33], M. Bruschi[6], P. Buchholz[11], M. Buchler[10], T. Buran[29], M. Capeáns[13], M. Capponi[6], J. Carvalho[8], J. Chamanina[27], B. X. Chen[4], R. Chistov[25], M. Chmeissani[2], A. Christensen[29], P. Conde[2], C. Cruse[11], M. Dam[9], K. M. Danielsen[29], M. Danilov[25], S. De Castro[6], H. Deckers[5], K. Dehmelt[13], H. Deppe[16], B. Dolgoshein[27], X. Dong[3], H. B. Dreis[16], M. Dressel[28], D. Dujmic[1], R. Eckmann[1], V. Egorytchev[13], K. Ehret[15,11], V. Eiges[25], F. Eisele[16], D. Emeliyanov[13], S. Erhan[22], S. Essenov[25], L. Fabbri[6], P. Faccioli[6], W. Fallot-Burghardt[15], M. Feuerstack-Raible[16], J. Flammer[13], H. Fleckenstein[13], B. Fominykh[25], S. Fourletov[27], T. Fuljahn[13], M. Funcke[11], D. Galli[6], A. Garcia[2], Ll. Garrido[2], D. Gascon[2], A. Gellrich[34,5,13], K. E. K. Gerndt[13], B. Giacobbe[6], J. Gläß[24], T. Glebe[15], D. Goloubkov[13,39], A. Golutvin[25], I. Golutvin[26], I. Gorbounov[31], A. Gorišek[19], O. Gouchtchine[25], D. C. Goulart[7], S. Gradl[16], W. Gradl[16], Yu. Guilitsky[25,13,41], T. Hamacher[13,1], J. D. Hansen[9], R. Harr[10], C. Hast[13], S. Hausmann[16], J. M. Hernández[13,34], M. Hildebrandt[16], A. Hölscher[16], K. Höpfner[13], W. Hofmann[15], M. Hohlmann[13], T. Hott[16], W. Hulsbergen[33], U. Husemann[11], O. Igonkina[25], M. Ispiryan[17], S. İssever[11], H. Itterbeck[13], J. Ivarsson[23,34], T. Jagla[15], Y. Jia[3], C. Jiang[3], A. Kaoukher[27,30], H. Kapitza[11], S. Karabekyan[13,44], P. Karchin[10], N. Karpenko[26], Z. Ke[3], S. Keller[31], F. Khasanov[25], H. Kim[1], Yu. Kiryushin[26], I. Kisel[28], F. Klefenz[15], K. T. Knöpfle[15], V. Kochetkov[25], H. Kolanoski[5], S. Korpar[21,19], C. Krauss[16], P. Kreuzer[22,13], P. Križan[20,19], D. Krücker[5], T. Kvaratskheliia[25], A. Lange[31], A. Lanyov[26], K. Lau[17], G. Leffers[15], I. Legrand[34], B. Lewendel[13], Y. Q. Liu[4], T. Lohse[5], R. Loke[5], B. Lomonosov[13,38], J. Lüdemann[13], R. Männer[24], R. Mankel[5], U. Marconi[6], S. Masciocchi[28], I. Massa[6], I. Matchikhilian[25], G. Medin[5], M. Medinnis[13,22], M. Mevius[32], A. Michetti[13], Yu. Mikhailov[25,13,41], R. Miquel[2], R. Mizuk[25], A. Mohapatra[7], A. Moshkin[26], B. Moshous[28], R. Muresan[9], S. Nam[10], M. Negodaev[13,38], I. Négri[13], M. Nörenberg[13], S. Nowak[34], M. T. Núñez Pardo de Vera[13], T. Oest[14,13], A. Oliveira[8], M. Ouchrif[32,33], F. Ould-Saada[29], C. Padilla[13], P. Pakhlov[25], Yu.Pavlenko[18], D. Peralta[2], R. Pernack[30], T. Perschke[28], R. Pestotnik[19], B. AA. Petersen[9], M. Piccinini[6], M. A. Pleier[15], M. Poli[37], V. Popov[25], A. Pose[34], D. Pose[26,16], V. Pugatch[15,18], Y. Pylypchenko[29], J. Pyrlik[17], S. Ramachandran[17], F. Ratnikov[13,25], K. Reeves[1,15], D. Reßing[13], K. Riechmann[28], J. Rieling[15], M. Rietz[28], I. Riu[13], P. Robmann[35], J. Rosen[12], Ch. Rothe[13], W. Ruckstuhl[33,†], V. Rusinov[25], V. Rybnikov[13], D. Ryzhikov[13,40], F. Saadi-Lüdemann[13], D. Samtleben[14], F. Sánchez[13,15], M. Sang[28], V. Saveliev[27], A. Sbrizzi[33], S. Schaller[28], P. Schlein[22], M. Schmelling[15], B. Schmidt[13,16], S. Schmidt[9], W. Schmidt-Parzefall[14], A. Schreiner[34], H. Schröder[13,30], H.D. Schultz[13], U. Schwanke[34], A. J. Schwartz[7], A. S. Schwarz[13], B. Schwenninger[11], B. Schwingenheuer[15], R. Schwitters[1], F. Sciacca[15], S. Semenov[25], N. Semprini-Cesari[6], E. Sexauer[15], L. Seybold[15], J. Shiu[10], S. Shuvalov[25,5], I. Siccama[13], D. Škrk[19], L. Sözüer[13], A. Soldatov[25,13,41], S. Solunin[26], A. Somov[5,13], S. Somov[13,39], V. Souvorov[34], M. Spahn[15], J. Spengler[15], R. Spighi[6], A. Spiridonov[34,25], S. Spratte[11], A. Stanovnik[20,19], M. Starič[19], R. StDenis[28,15], C. Stegmann[34,5], S. Steinbeck[14], O. Steinkamp[33], D. Stieler[31], U. Straumann[16], F. Sun[34], H. Sun[3], M. Symalla[11], S. Takach[10], N. Tesch[13], H. Thurn[13], I. Tikhomirov[25], M. Titov[25], U. Trunk[15], P. Truöl[35], I. Tsakov[13,42], U. Uwer[5,16], V. Vagnoni[6], C. van Eldik[11], R. van Staa[14], Yu. Vassiliev[18,11], M. Villa[6], A. Vitale[6], I. Vukotic[5], G. Wagner[13], W. Wagner[28], H. Wahlberg[32], A. H. Walenta[31], M. Walter[34], T. Walter[35], J. J. Wang[4], Y. M. Wang[4], R. Wanke[15], D. Wegener[11], U. Werthenbach[31], P. J. Weyers[5], H. Wolters[8], R. Wurth[13], A. Wurz[24], S. Xella-Hansen[9], J. Yang[4], Yu. Zaitsev[25], M. Zavertyaev[15,38], G. Zech[31], T. Zeuner[31], A. Zhelezov[25], Z. Zheng[3], Z. Zhu[3], R. Zimmermann[30], T. Živko[19], A. Zoccoli[6], J. Zweizig[13,22]

[1] Department of Physics, University of Texas, Austin, TX 78712-1081, USA[a]
[2] Department ECM, Faculty of Physics, University of Barcelona, 08028 Barcelona, Spain [b]
[3] Institute for High Energy Physics, Beijing 100039, P.R. China
[4] Institute of Engineering Physics, Tsinghua University, Beijing 100084, P.R. China

[a] supported by the U.S. Department of Energy (DOE)
[b] supported by the CICYT contract AEN99-0483

[5] Institut für Physik, Humboldt-Universität zu Berlin, 10115 Berlin, Germany [c]
[6] Dipartimento di Fisica dell' Università di Bologna and INFN Sezione di Bologna, 40126 Bologna, Italy
[7] Department of Physics, University of Cincinnati, Cincinnati, Ohio 45221, USA[a]
[8] LIP Coimbra and Lisboa, 3004-516 Coimbra, Portugal [d]
[9] Niels Bohr Institutet, 2100 Copenhagen, Denmark [e]
[10] Department of Physics and Astronomy, Wayne State University, Detroit, MI 48202, USA[a]
[11] Institut für Physik, Universität Dortmund, 44227 Dortmund, Germany[c]
[12] Northwestern University, Evanston, Il 60208, USA[a]
[13] DESY, 22603 Hamburg, Germany
[14] Institut für Experimentalphysik, Universität Hamburg, 22761 Hamburg, Germany[c]
[15] Max-Planck-Institut für Kernphysik, 69117 Heidelberg, Germany[c]
[16] Physikalisches Institut, Universität Heidelberg, 69120 Heidelberg, Germany[c]
[17] Department of Physics, University of Houston, Houston, TX 77204, USA[a,f]
[18] Institute for Nuclear Research, Ukrainian Academy of Science, 03680 Kiev, Ukraine [g]
[19] J. Stefan Institute, 1001 Ljubljana, Slovenia
[20] University of Ljubljana, 1001 Ljubljana, Slovenia
[21] University of Maribor, 2000 Maribor, Slovenia
[22] University of California, Los Angeles, CA 90024, USA[h]
[23] Lund University, 22362 Lund, Sweden
[24] Lehrstuhl für Informatik V, Universität Mannheim, 68131 Mannheim, Germany
[25] Institute of Theoretical and Experimental Physics, 117259 Moscow, Russia[g,i]
[26] Joint Institute for Nuclear Research Dubna, 141980 Dubna, Moscow region, Russia
[27] Moscow Physical Engineering Institute, 115409 Moscow, Russia
[28] Max-Planck-Institut für Physik, Werner-Heisenberg-Institut, 80805 München, Germany[c]
[29] Dept. of Physics, University of Oslo, 0316 Oslo, Norway[j]
[30] Fachbereich Physik, Universität Rostock, 18051 Rostock, Germany[c]
[31] Fachbereich Physik, Universität Siegen, 57068 Siegen, Germany[c]
[32] Universiteit Utrecht/NIKHEF, 3584 CB Utrecht, The Netherlands [k]
[33] NIKHEF, 1009 DB Amsterdam, The Netherlands[k]
[34] DESY Zeuthen, 15738 Zeuthen, Germany
[35] Physik-Institut, Universität Zürich, 8057 Zürich, Switzerland [l]
[36] Brookhaven National Laboratory, Upton, NY 11973, USA
[37] visitor from Dipartimento di Energetica dell' Università di Firenze and INFN Sezione di Bologna, Italy
[38] visitor from P.N. Lebedev Physical Institute, 117924 Moscow B-333, Russia
[39] visitor from Moscow Physical Engineering Institute, 115409 Moscow, Russia
[40] visitor from Institute of Nuclear Power Engineering, 249030, Obninsk, Russia
[41] visitor from Institute for High Energy Physics, Protvino, Russia
[42] visitor from Institute for Nuclear Research, INRNE-BAS, Sofia, Bulgaria
[43] visitor from High Energy Physics Institute, 380086 Tbilisi, Georgia
[44] visitor from Yerevan Physics Institute, Yerevan, Armenia

Received: 6 June 2002 / Revised version: 2 September 2002 /
Published online: 8 November 2002 –

Abstract. Using the HERA – B detector, the $b\bar{b}$ production cross section has been measured in 920 GeV proton collisions on carbon and titanium targets. The $b\bar{b}$ production was tagged via inclusive bottom quark decays into J/ψ by exploiting the longitudinal separation of $J/\psi \to l^+l^-$ decay vertices from the primary proton-nucleus interaction. Both e^+e^- and $\mu^+\mu^-$ channels have been reconstructed and the combined analysis yields the cross section $\sigma(b\bar{b}) = 32^{+14}_{-12}(\text{stat})\,^{+6}_{-7}(\text{sys})$ nb/nucleon.

[c] supported by the Bundesministerium für Bildung und Forschung, FRG, under contract numbers 05-7BU35I, 05-7DO55P, 05 HB1HRA, 05 HB1KHA, 05 HB1PEA, 05 HB1PSA, 05 HB1VHA, 05 HB9HRA, 05 7HD15I, 05 7HH25I, 05 7MP25I, 05 7SI75I
[d] supported by the Portuguese Fundação para a Ciência e Tecnologia
[e] supported by the Danish Natural Science Research Council
[f] supported by the Texas Advanced Research Program
[g] supported by the National Academy of Science and the Ministry of Education and Science of Ukraine
[h] supported by the U.S. National Science Foundation Grant PHY-9986703
[i] supported by the Russion Fundamental Research Foundation under grant RFFI-00-15-96584 and the BMBF via the Max Planck Research Award
[j] supported by the Norwegian Research Council
[k] supported by the Foundation for Fundamental Research on Matter (FOM), 3502 GA Utrecht, The Netherlands
[l] supported by the Swiss National Science Foundation

1 Introduction

The theoretical description of heavy quark hadroproduction in fixed target experiments has been a subject of great attention in recent years [1–4]. The predictions, based on perturbative QCD, are compatible with experimental results from pion and proton beams, but both theoretical and experimental uncertainties are large. Only two measurements of the $b\bar{b}$ production cross section in proton-nucleus $p+A$ interactions were previously reported [5,6].

The HERA – B experiment is designed to identify B-meson decays in a dense hadronic environment, with a large geometrical coverage. Interactions are produced on target wires in the halo of the 920 GeV HERA proton beam. The $b\bar{b}$ production cross section (σ_B^A) on a nucleus of atomic number A is obtained from the inclusive reaction

$$pA \to b\bar{b}\,X \quad \text{with} \quad b\bar{b} \to J/\psi\,Y \to (e^+e^-/\mu^+\mu^-)Y. \quad (1)$$

The b-hadron decays into J/ψ ("$b \to J/\psi$" in the following) are distinguished from the large prompt J/ψ background by exploiting the b lifetime in a detached vertex analysis. We select $b \to J/\psi \to l^+l^-$ decays in both the muon and electron channels and perform a combined $b\bar{b}$ production cross section measurement.

In order to minimize the systematic errors related to detector and trigger efficiencies and to remove the dependence on the absolute luminosity determination, the measurement is performed relative to the known prompt J/ψ production cross section σ_P^A [7,8]. Our measurement covers the J/ψ Feynman-x (x_F) range $-0.25 \le x_F \le 0.15$. Within our acceptance, the b to prompt cross section ratio can be expressed as:

$$\frac{\Delta\sigma_B^A}{\Delta\sigma_P^A} = \frac{N_B}{N_P}\,\frac{1}{\varepsilon_R\,\varepsilon_B^{\Delta z}\,\mathrm{Br}(b\bar{b}\to J/\psi X)}\ , \quad (2)$$

where $\Delta\sigma_B^A$ and $\Delta\sigma_P^A$ are the $b \to J/\psi$ and prompt J/ψ cross sections limited to the mentioned x_F range, N_B and N_P are the observed number of detached $b \to J/\psi$ and prompt J/ψ decays. ε_R is the relative detection efficiency of $b \to J/\psi$ with respect to prompt J/ψ, including contributions from the trigger, the dilepton reconstruction and the J/ψ vertexing. $\varepsilon_B^{\Delta z}$ is the efficiency of the detached vertex selection. The branching ratio $\mathrm{Br}(b\bar{b}\to J/\psi X)$ in hadroproduction is assumed to be the same as that measured in Z decays, with the value $2\cdot(1.16\pm0.10)\%$ [9].

The prompt J/ψ production cross section per nucleon, $\sigma(pN \to J/\psi X) = \sigma_P^A/A^\alpha$, was previously measured by two fixed target experiments [7,8]. After correcting for the most recent measurement of the atomic number dependence ($\alpha = 0.955 \pm 0.005$ [10]) and rescaling [11] to the HERA – B c.m.s. energy, $\sqrt{s} = 41.6$ GeV, we obtain a reference prompt J/ψ cross section of $\sigma(pN \to J/\psi X) = (357\pm8(\mathrm{stat})\pm27(\mathrm{sys}))$ nb/nucleon. About 70% [7] of the J/ψ are produced in the kinematic range covered by our measurement.

Since no nuclear suppression has been observed in D-meson production [12] and a similar behavior is expected in the b channel [13], we assume $\alpha = 1.0$ for the $b\bar{b}$ production cross section results presented here; i.e., $\sigma_B^A = \sigma(pN \to b\bar{b})\cdot A$.

2 Detector, trigger and data sample

A side view of the HERA – B [14,15] spectrometer is shown in Fig. 1. The spectrometer has a large geometrical coverage, from 15 mrad to 220 mrad in the bending plane and from 15 mrad to 160 mrad in the vertical plane.

The target assembly [16] consists of two wire stations separated by 4 cm along the beam line, each containing 4 target wires of different materials. A servo system automatically steers the target wires during a run in order to maintain a constant interaction rate. The Vertex Detector System (VDS) [17] is realized by a system of 20 Roman pots containing seven planar stations (4 stereo views) of double-sided silicon micro-strip detectors (50 mm × 70 mm sensitive area, 50 μm pitch) that are operated in a vacuum vessel at 10 to 15 mm distance from the proton beam. An additional station is mounted immediately behind the 3 mm thick Al window of the vacuum vessel.

A dipole magnet with 2.13 Tm field-integral houses a first set of tracking stations, followed by a second set extending to 13 m downstream of the interaction region. To cope with the large particle flux gradient radial to the beam, the tracker is divided into a fine grained Inner Tracker (ITR) [18] and a large area Outer Tracker (OTR) [14,19]. The ITR uses micro-strip gas chambers (typical pitch of 300 μm) with gas electron multipliers. The OTR uses honeycomb drift cells with wire pitches of 5 mm near the beam and 10 mm away from the beam.

The particle identification is performed by a ring imaging Cherenkov hodoscope (RICH) [20], an electromagnetic calorimeter (ECAL) [21] and a muon detector (MUON) [22]. The RICH detector uses C_4F_{10} as radiator. The focal planes of the detector (above and below the beam line, respectively) are read out by multianode photomultipliers. The ECAL is based on "shashlik" sampling calorimeter technology, consisting of scintillator layers sandwiched between metal absorbers. In the radially innermost section, W is used in the absorber, and Pb everywhere else. The MUON system consists of 4 tracking stations located in the most downstream portion of the detector, at different depths in iron and iron-loaded absorbers. It is built from gas-pixel chambers in the radially innermost region and from proportional tube chambers, some with segmented cathodes (pads), everywhere else.

The data sample presented in this analysis was acquired in a short physics run during the HERA – B commissioning period in summer 2000, at ≈5 MHz interaction rate, with a maximum of two target wires operated simultaneously and separated by 4 cm along the beam direction. The two wires were made of carbon (1000 μm longitudinally and 100 μm transversely) and titanium (500 μm and 50 μm, respectively).

The data were collected by triggering on dimuon and dielectron signatures. The MUON pretrigger candidates were based on a double pad chamber coincidence [23],

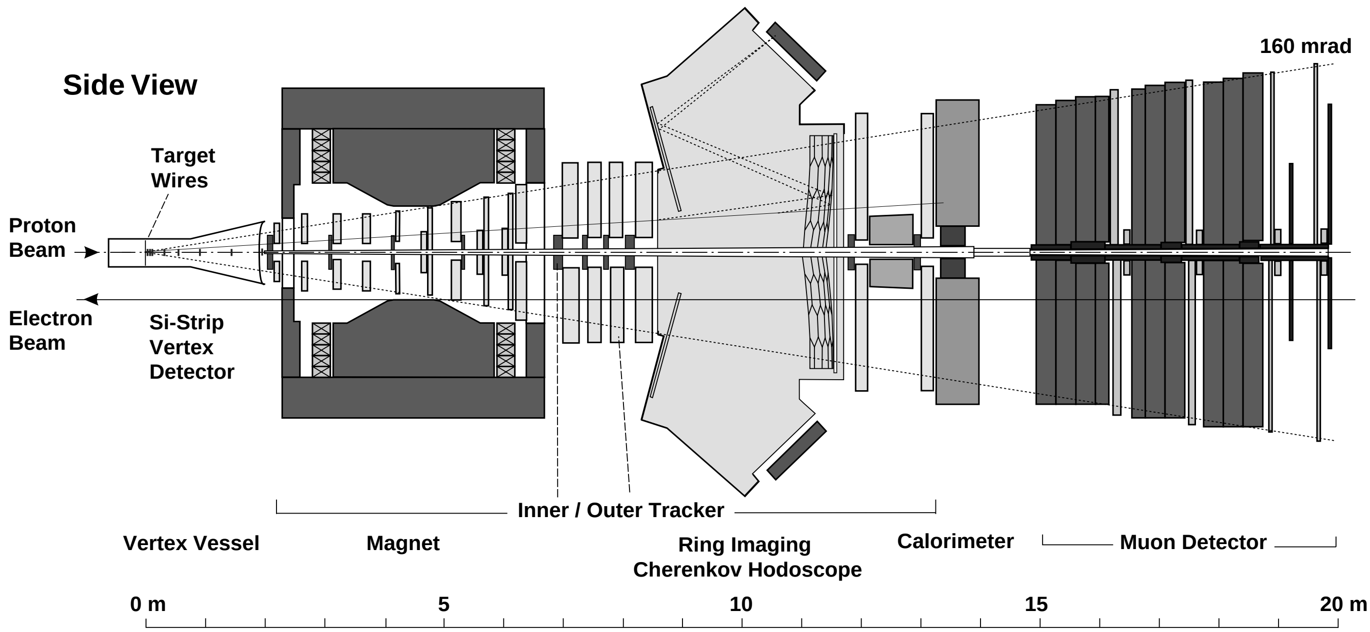

Fig. 1. Side view of the HERA – B detector

while the ECAL pretrigger candidates were defined by ECAL clusters with a transverse energy $E_T > 1.0$ GeV [24]. The First Level Trigger (FLT) required two pretrigger candidates of the same type and forwarded these to the Second Level Trigger (SLT). The SLT is a software filter [25] running on a farm of 240 PCs. Starting from the pad coincidences and high-E_T ECAL clusters, a fast hit-counting algorithm and a simplified Kalman filter were applied to the OTR and VDS data to confirm the lepton pair candidates. An invariant mass cut of $M > 2.0$ GeV/c^2 and an unlike-sign track requirement were also applied in the electron channel. The data from accepted events were assembled and sent to the online reconstruction farm [26], consisting of 100 dual-CPU PCs. The whole trigger chain allowed a reduction of the initial interaction rate of 5 MHz to a final output rate of 20 Hz [27]. A total of ≈450,000 dimuon and ≈900,000 dielectron candidates were recorded under these conditions.

At the time of data taking, the ITR and the MUON pixel chambers were not included in the trigger. As a consequence, the forward hemisphere of the proton-nucleus c.m.s. is reduced in this measurement, compared to the full HERA – B acceptance.

3 Monte Carlo simulation

A Monte Carlo (MC) simulation is used to determine the efficiency terms in (2) and to estimate the prompt J/ψ background contribution to the $b \to J/\psi$ decay channel.

The simulation of heavy quark (Q) production is achieved, first, by generating the basic process $pN \to Q\bar{Q}X$ including hadronization, using the Pythia 5.7 event generator [28]; secondly, the remaining part of the process (X) is given as an input to the Fritiof 7.02 package [29] to simulate further interactions inside the nucleus.

To describe the prompt J/ψ kinematics accurately, the generated events are weighted according to the known prompt J/ψ differential cross sections ($d\sigma/dp_T^2$ and $d\sigma/dx_F$) measured in proton-gold collisions [7]. These results were obtained in the positive x_F region, while our measurement covers the range $-0.25 \leq x_F \leq 0.15$. MC studies based on the Color Octet Model [30] of charmonium production show a symmetric x_F distribution of prompt J/ψ decays. We therefore use the experimental parameterization [7] to extrapolate to the full x_F space. The model dependence of the generated p_T spectrum is of less importance since our J/ψ p_T acceptance is essentially flat in the relevant range. Possible effects of the prompt J/ψ polarization have been studied and are included in the systematic errors of our prompt J/ψ MC model.

For the $b\bar{b}$ MC simulations, the events generated by Pythia are weighted according to a model with various contributions. First, the generated b quark kinematics (x_F and p_T) are given by the computation of M. Mangano et al. [31] using the most recent next-to-next-to-leading-logarithm (NNLL) MRST parton distribution functions [32] with a b quark mass of $m_b = 4.75$ GeV/c^2 and a QCD renormalization scale $\mu = \sqrt{m_b^2 + p_T^2}$. Second, the intrinsic transverse momenta of the colliding quarks are smeared with a Gaussian distribution leading to $\langle k_T^2 \rangle = 0.5$ GeV^2/c^2 [33]. Finally, the b fragmentation is described by a Peterson function [34] with a parameter $\epsilon = 0.006$ [5]. The subsequent b-hadron production and decay are controlled by the Pythia default parameters. The b-hadron average lifetime is taken from [9]: $\tau_b = 1.564 \pm 0.014$ ps.

The sensitivity of the final result on the $b\bar{b}$ cross section within our acceptance ($\Delta\sigma(b\bar{b})$) has been determined by varying the following $b\bar{b}$ MC model parameters: the parton distribution functions (from MRST to CTEQ5 [35]), the b quark mass (in the range $m_b \in [4.5, 5.0]$ GeV/c^2),

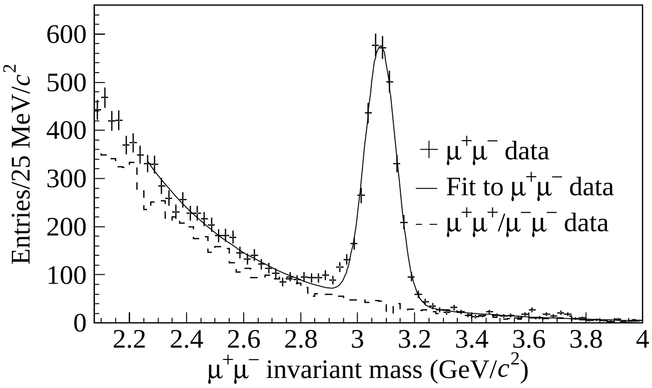

Fig. 2. The $\mu^+\mu^-$ invariant mass spectrum, after the J/ψ selection cuts. The fit (*solid line*) assumes a Gaussian signal and an exponential background. The like-sign spectrum (*dashed line*) shows small discrepancies in the background regions (see text); it is not used in the analysis and serves only for illustration purposes

the QCD renormalization scale (from $0.5\sqrt{m_b^2 + p_T^2}$ to $2\sqrt{m_b^2 + p_T^2}$), the fragmentation function (from the Peterson form [5,36,37] with parameter $\epsilon \in [0.002, 0.008]$, to the Kartvelishvili form [38] with parameter $\alpha_\beta = 13.7 \pm 1.3$ [37]), the intrinsic transverse momentum distribution (with $\langle k_T^2 \rangle$ in the range [0.125, 2.0] GeV^2/c^2) and the fraction of b-baryons produced in the b hadronization process in the range [0, 12]%. The observed variations in the detection efficiencies have been included in the systematic error. No significant dependence ($< 1.5\%$) of the cross section has been found on the momentum of the J/ψ mesons in the b-hadron rest frame and on the J/ψ polarization.

The generated particles are propagated through the geometry and material description of the detector using the Geant 3.21 package [39]. A simulation of the detector response to particles is achieved by reproducing the digitization of electronic signals, with a realistic description of hit efficiencies and problematic channels. The MC events are subjected to a full trigger simulation and reconstructed with the same algorithms as the data.

4 J/ψ event selection

Since the observed number of prompt J/ψ decays is used as a normalization factor of the $b\bar{b}$ cross section measurement, we begin by selecting and counting the number of J/ψ decays (N_P), before applying the detached vertex analysis. The lepton reconstruction in the OTR is seeded with the dilepton trigger track candidates; moreover a matching criteria is applied between the reconstructed track and the trigger track candidate in both the OTR and the VDS. The J/ψ selection is completed with a dilepton vertex search, based on a χ^2 minimization algorithm (typically $\chi^2 \leq 5$ for 1 degree of freedom) and with Particle Identification cuts (PID) as described below. The $J/\psi \to l^+l^-$ selection and counting procedure differs between the muon and electron channels, due to differences in the background levels, shapes and triggering conditions.

4.1 $J/\psi \to \mu^+\mu^-$

Three criteria are used to select $J/\psi \to \mu^+\mu^-$ decays and to purify the reconstructed sample from non-J/ψ background: a dimuon vertex requirement and muon identification cuts in both the MUON and the RICH systems. The cuts are chosen to give the best signal significance ($S/\sqrt{B}$) on the number of seen J/ψ (S) with the observed background (B). The resulting spectrum is shown in Fig. 2, with $N_P = 2880 \pm 60$ prompt $J/\psi \to \mu^+\mu^-$ decays. The like-sign spectrum shown in Fig. 2 is obtained from the same set of triggered events: the small discrepancy in number of reconstructed events in the background regions arises from the difference in trigger acceptance between the two cases and from physics contributions to the unlike-sign spectrum (Drell-Yan, open charm production).

4.2 $J/\psi \to e^+e^-$

The selection of $J/\psi \to e^+e^-$ decays is more complex due to very large background contributions, mainly from pions interacting in the ECAL and hadrons overlapping with energetic neutral showers. Due to such background, a clear J/ψ signal can be reconstructed only by means of strong electron identification requirements. Electron identification in the ECAL is based both on the ratio of the cluster energy E to the momentum p from tracking (E/p) and on the search for electron bremsstrahlung signals:

– the E/p distribution is established for a purified $J/\psi \to e^+e^-$ sample by using a double-bremsstrahlung requirement as described in the following paragraph. The E/p spectrum is compatible with a Gaussian distribution of mean 1.00 and width $\sigma \approx 9\%$;
– bremsstrahlung photons emitted upstream of the magnet maintain the original electron direction; thus they can be used to correct the electron momentum at the vertex and they also provide a clean electron signature (bremsstrahlung tag).

The e^+e^- invariant mass distribution is shown in Fig. 3a, requiring only that E/p be within 1 σ from unity for each track. Figures 3b,c show the improvements in signal significance that are obtained when the bremsstrahlung selection is added to the E/p requirement.

Table 1 lists the number of prompt J/ψ signal events found for different E/p and bremsstrahlung requirements. Using these J/ψ sets one can measure the bremsstrahlung tag probability for a single electron redundantly, resulting in an average $\epsilon_{\mathrm{brems}} = 0.34 \pm 0.02(\mathrm{stat}) \pm 0.02(\mathrm{sys})$. The systematic uncertainties include the observed fluctuations when varying the fitting functions and range used to estimate the amount of J/ψ events in the invariant mass spectra.

The same analysis, performed on MC data, yields a MC tag probability of $\epsilon_{\mathrm{brems}}^{MC} = 0.34 \pm 0.01(\mathrm{stat}) \pm 0.01(\mathrm{sys})$ in good agreement with the measured value. This gives further confidence in the quality of our detector description and MC simulation, in particular in the delicate region before the magnet, where the triggered electrons cross

Table 1. The number of prompt $J/\psi \to e^+e^-$ with different bremsstrahlung requirements and different E/p cuts on both tracks. The bremsstrahlung tag probability for a single electron is reported for each E/p cut. The value at 3σ in square brackets is obtained by extrapolation from samples with stronger electron identification cuts (see text)

Bremsstrahlung requirement	E/p cut in units of σ 0.5σ	1σ	2σ	3σ
None	895 ± 75	2553 ± 184	5362 ± 292	$[5710 \pm 380 \pm 280]$
≥ 1	$519 \pm 45 \pm 11$	$1420 \pm 70 \pm 48$	$2851 \pm 108 \pm 48$	$3304 \pm 148 \pm 188$
2	$106 \pm 13 \pm 2$	$308 \pm 24 \pm 6$	$587 \pm 38 \pm 14$	$661 \pm 40 \pm 29$
ϵ_{brems}	$0.34 \pm 0.03 \pm 0.01$	$0.35 \pm 0.02 \pm 0.01$	$0.33 \pm 0.02 \pm 0.01$	$0.33 \pm 0.02 \pm 0.02$

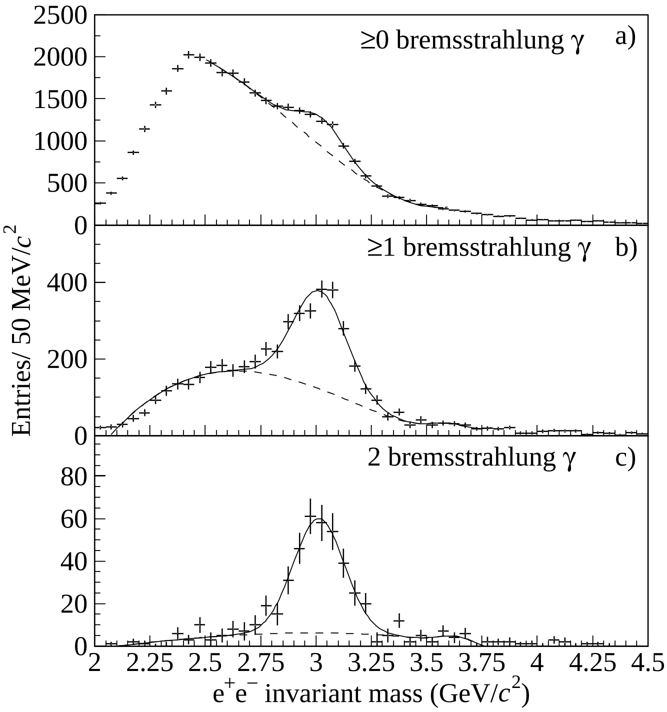

Fig. 3a–c. The e^+e^- invariant mass spectra, with an E/p cut at 1 σ on both e^+ and e^- tracks; **a** no bremsstrahlung requirement; **b** with at least 1 identified bremsstrahlung photon; **c** with two identified bremsstrahlung photons. The fits (*solid lines*) assume a Gaussian signal and a polynomial shape for the background. The background shapes (*dashed lines*) differ from the dimuon case (Fig. 2), due to E_T and invariant mass cuts in the trigger

about 0.07 radiation lengths of material. Due to the geometry and trigger requests, energetic bremsstrahlung photons emitted in this region point to the calorimeter and have a reconstruction efficiency of $(85 \pm 2)\%$, limited by photon conversions before the end of the magnet region and by non-working channels.

The good knowledge of the particle identification efficiencies allows us to infer the number of prompt J/ψ present in a sample where looser identification cuts have been applied and where no clear J/ψ signal is directly visible. Under such conditions, the normalization factor N_P can be obtained while preserving reasonable statistics

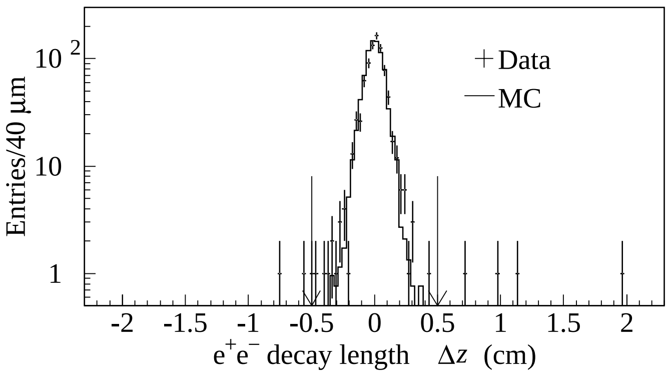

Fig. 4. The decay length (Δz) of purified $J/\psi \to e^+e^-$ events (2 bremsstrahlung sample, $\approx 15\%$ background) for real data and compared to MC prompt J/ψ events. The resolutions of both data and MC distributions are in agreement (715 ± 24 μm and 721 ± 10 μm, respectively). The arrows mark the cuts applied in the detached vertex analysis

for the final detached vertex analysis, which relies only on the vertex separation cuts for the background rejection, as will be shown in Sect. 5.

The total number of prompt J/ψ in our sample with no bremsstrahlung tag requirement and with a 3σ E/p cut is $N_P = 5710 \pm 380(\text{stat}) \pm 280(\text{sys})$ (entry in square brackets in Table 1).

5 Detached vertex analysis

The long decay length of b-hadrons is used to separate the $b \to J/\psi$ events from the prompt J/ψ and to further reduce the non-J/ψ background. The decay length (Δz), defined as the distance along the beam axis between the J/ψ decay vertex and the closest wire (primary production point), is shown in Fig. 4 for a purified sample of $J/\psi \to e^+e^-$ events (2 bremsstrahlung requirement). The r.m.s. resolution in decay length is smaller than one-tenth the mean decay length of triggered b-hadrons ($\approx$0.8 cm). Given the achieved vertex resolution, a detached vertex cut proves to be efficient in the signal selection. Additionally, cuts on the minimum impact parameter of both leptons to the production vertex (I_v) and to the wire (I_w) are applied in the detached vertex selection. Both impact parameter cuts are needed, since the 2-dimensional

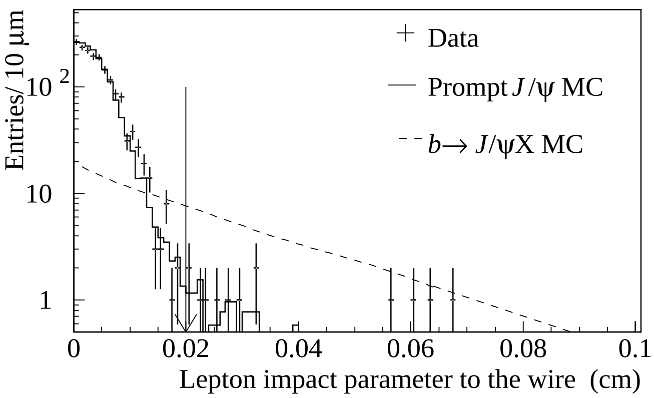

Fig. 5. The minimal impact to the wire (I_w) of the two lepton tracks for purified $J/\psi \to e^+e^-$ events (2 bremsstrahlung sample) data and in MC for $J/\psi \to e^+e^-$ events. The expected shape from $b \to J/\psi$ decays is shown in dashed line (arbitrary scale). The arrow marks the cut applied in the e^+e^- detached event selection

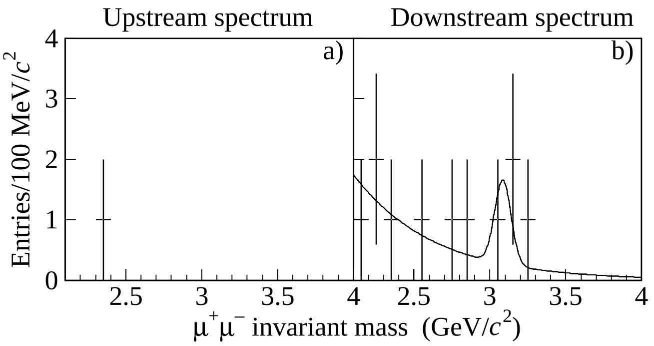

Fig. 6a,b. The upstream **a** and downstream **b** invariant $\mu^+\mu^-$ mass spectrum after detached event selection. The downstream curve shows the result of the unbinned likelihood fit, in which the yields of background and signal contributions, as defined in the text, were left as free parameters

I_v cut gives the best separation between the signal and the prompt background, whereas the I_w cut can additionally suppress background tracks originating from other potential primary vertices on the same wire. In the electron channel the I_v cut is replaced by an "isolation cut", as explained in more details in Sect. 5.2. The minimum impact parameter distribution of prompt $J/\psi \to e^+e^-$ decay leptons (purified sample) to the wire is compared to the corresponding distribution from $b \to J/\psi$ decay leptons (dashed line) in Fig. 5, illustrating the potential gain in $b \to J/\psi$ signal-purity when applying a minimum impact parameter cut.

The prompt J/ψ which survive the detached vertex cuts cannot be distinguished from $b \to J/\psi$ events and their contribution to the detached b signal has to be determined from MC. A study has been performed to ensure that the simulation tool reliably reproduces the real data for the physical quantities defining the detached selection cuts, as illustrated by the good MC-data agreement in Fig. 4 and Fig. 5. In the simulation of the $\mu^+\mu^-$ channel, the standard MC track slopes have been smeared according to a Gaussian distribution, increasing the slope errors by 20% on average, in order to match the hit resolution observed in data; this smearing procedure is of small relevance in the detached vertex analysis, given the loose cut values compared to the observed vertex resolutions.

The optimization of the detached vertex cuts is achieved by maximizing the ratio $S/\sqrt{B}$, S being the number of accepted signal events in the MC $b \to J/\psi$ sample and B the number of background events in real data, observed in the whole upstream region and downstream in the side bins of the J/ψ invariant mass signal. The systematic errors in the final $\sigma(b\bar{b})$ result take into account the variations in the signal estimated under different sets of cuts found by the optimization procedure.

The main background contributions expected in the detached sample are due to combinatorics (bad vertex or track reconstruction) and to double semileptonic $c\bar{c}$ or $b\bar{b}$ events. The combinatorial yield is estimated through the observed events in the region upstream of the primary interaction (unphysical region), while the charm background level is estimated by means of MC simulations, assuming a $c\bar{c}$ production cross section of 40 μb/nucleon for our 920 GeV proton beam energy [40]. The $b\bar{b}$ background yield is estimated by studying the MC mass spectrum of $b\bar{b}$ events surviving trigger and selection cuts, with a contribution relative to the observed yield of $b \to J/\psi \to l^+l^-$ events.

5.1 $b \to J/\psi \to \mu^+\mu^-$

The detached vertex cuts found by the optimization procedure in the dimuon channel are: a minimum decay length of 7.5 times the uncertainty on the secondary vertex position[1], a minimum track impact parameter to the assigned primary vertex of 160 μm and a minimum track impact parameter to the assigned wire of 45 μm.

Only 11 events survive these cuts downstream of the primary interaction region with invariant mass above 2.1 GeV/c^2 (see Fig. 6). Only a single event is found upstream of the primary interaction.

In order to use the full information of the detached invariant mass spectrum, an unbinned likelihood fit is performed, using the Gaussian parameters of the prompt J/ψ signal together with an exponential background contribution with free slope. The output of the fit shown in Fig. 6 yields $1.9^{+2.2}_{-1.5}$ $b \to J/\psi$ events. The background slope obtained from the fit is compatible with the simulated charm and bottom quark background shape, although the statistics are low.

From simulation, the expected prompt J/ψ background is negligible. The estimated background contributions of semileptonic charm and bottom quark decays, together with the single event expected from combinatorial background (seen upstream) and the number of fitted signal events, are compatible with the 11 events observed downstream of the primary interaction region.

[1] The typical cutoff is at about 0.5 cm, with some events down to 0.3 cm being accepted

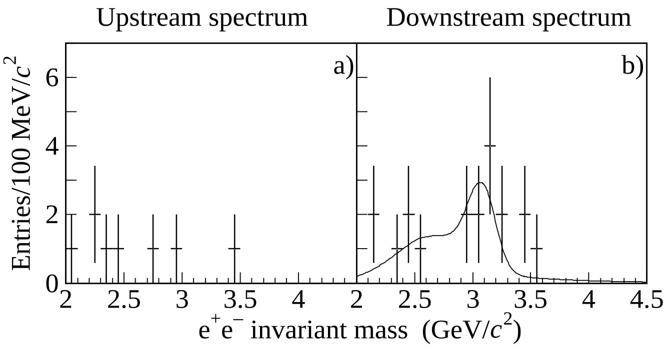

Fig. 7a,b. The upstream **a** and downstream **b** e^+e^- invariant mass spectra after the detached event selection. The downstream curve shows the result of the unbinned likelihood fit, in which the yields of background and signal contributions, as defined in the text, were left as free parameters

To determine $\Delta\sigma(b\bar{b})$ in our x_F range, the prompt J/ψ and $b \to J/\psi$ MC events are submitted to the same analysis chain used for real data. From simulation we obtain the efficiency terms entering in the cross section formula: $\varepsilon_R \cdot \varepsilon_B^{\Delta z} = 0.41 \pm 0.01$. The corresponding $b\bar{b}$ cross section measured in the $\mu^+\mu^-$ channel is $\Delta\sigma(b\bar{b}) = \sigma_B^A/A = 16^{+18}_{-12}$ nb/nucleon, obtained by using the weighted average of our target materials. All parameters contributing to the measurement (2) are summarized in Table 2.

5.2 $b \to J/\psi \to e^+e^-$

The cut optimization procedure in the e^+e^- channel results in the following criteria: a minimum decay length of 0.5 cm, a minimum track impact parameter to the assigned wire of 200 μm or alternatively an isolation of the lepton candidate at the z of the wire from any other track by a minimum distance of 250 μm. The "isolation cut" plays almost the same role as the I_v cut in the muon channel analysis, but with a less stringent efficiency requirement. The differences in types and values of the detached selection cuts between the muon and electron analysis are due to the very different background conditions.

The detached selection yields 8 events upstream of the primary interaction region (pure combinatorial background) and 19 downstream events (see Fig. 7). Among the downstream candidates, 10 events are found in the J/ψ mass window (2.8 GeV/c^2 $< m_{e^+e^-} <$ 3.3 GeV/c^2).

Similarly to the muon analysis, an unbinned likelihood fit is performed on the invariant mass spectrum of the detached downstream e^+e^- candidates. The shape of the signal is taken from simulated $b \to J/\psi$ decays, while the background shape is a combination of the shapes obtained from simulated double semileptonic bottom quark decays and from pure combinatorial (upstream) events. The result of the likelihood fit is shown in Fig. 7b, yielding $8.6^{+3.9}_{-3.2}$ $b \to J/\psi$ events. When the background shape used in the fit is replaced by a pure combinatorial background shape or by a pure double semileptonic $b\bar{b}$ background, a $\pm 7\%$ variation is observed in the number of $b \to J/\psi$ events.

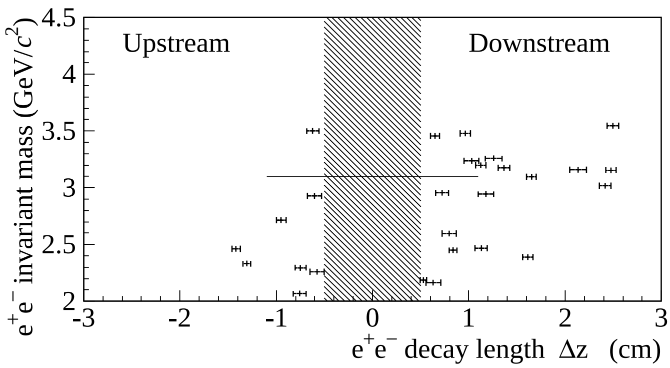

Fig. 8. The scatter plot of e^+e^- invariant masses versus the measured decay length (Δz) for the selected detached events. The shaded region is removed by the Δz cut. The horizontal line shows the mean J/ψ invariant mass value. A clear clustering of events around the J/ψ mass with large Δz is observed in the downstream sample

Table 2. The parameters entering into the $\sigma(b\bar{b})$ measurement (2). The covered J/ψ kinematic range is: $-0.25 < x_F < 0.15$

	$\mu^+\mu^-$ channel	e^+e^- channel
Target	77% C(A=12) + 23% Ti(A=48)	
Interaction rate	5 MHz	
Beam energy	920 GeV	
$\sqrt{s}$	41.6 GeV	
α	0.955 ± 0.005	
$\sigma(J/\psi)$	357 ± 28 nb/nucleon	
Prompt J/ψ (N_P)	2880 ± 60	5710 ± 380
Detached J/ψ (N_B)	$1.9^{+2.2}_{-1.5}$	$8.6^{+3.9}_{-3.2}$
$\varepsilon_R \cdot \varepsilon_B^{\Delta z}$	0.41 ± 0.01	0.44 ± 0.02
Br($b\bar{b} \to J/\psi X$)	$(2.32 \pm 0.20)\%$	
$\Delta\sigma(b\bar{b})$	16^{+18}_{-12} nb/nucl.	38^{+18}_{-15} nb/nucl.
Combined $\Delta\sigma(b\bar{b})$	30^{+13}_{-11}(stat) $\pm$ 6(sys) nb/nucleon	
Combined $\sigma(b\bar{b})$	32^{+14}_{-12}(stat) $^{+6}_{-7}$(sys) nb/nucleon	

This contribution is included in the systematic error of our measurement. Although a direct check on real data of the assumed shape of the signal is not possible due to the high background level, we have verified on samples with higher PID requirements ($\geq$ 1 bremsstrahlung tag and/or E/p cuts at $\leq 2\sigma$) that the $J/\psi \to e^+e^-$ shape obtained from simulations is compatible with real data.

The expected background from prompt J/ψ decays is of less than 0.2 events at the 90% C.L. in the whole downstream region. As in the $\mu^+\mu^-$ case, the estimated background yields from semileptonic charm and bottom quark decays, together with the expected combinatorial background level (8 events seen upstream) and the fitted signal, are compatible with the 19 events observed downstream of the primary interaction region.

A detailed study of the decay length (Δz) has been performed in order to confirm the b assignment. In Fig. 8, the selected detached events are displayed in a scatter plot of the invariant mass versus the measured decay length: a clustering is observed around the J/ψ invariant mass for large Δz values in the region downstream of the primary interaction. A mean decay length of 0.81 ± 0.03 cm on $b\bar{b}$ events is expected from MC. When an unbinned maximum likelihood fit is performed on Δz, we measure 1.0 ± 0.3 cm for the 10 downstream events in the J/ψ region (2.8 GeV$/c^2 < m_{e^+e^-} < 3.3$ GeV$/c^2$), in good agreement with the $b\bar{b}$ interpretation, while the 8 upstream background events yield a mean decay length of 0.36 ± 0.13 cm (measured using $-\Delta z$). To further verify that the selected events have features compatible with b decays, we performed a visual inspection of the candidates studying extra detached vertices (from the other b decay) and extra tracks attached to the J/ψ vertex. Both categories of events are observed, and their yields are compatible with MC expectations. Within the limits of the available statistics, the J/ψ x_F and p_T distributions are also compatible with the $b \to J/\psi$ interpretation.

From MC simulation, we obtain the efficiency terms entering in the cross section measurement (2): $\varepsilon_R \cdot \varepsilon_B^{\Delta z} = 0.44\pm0.02$. The corresponding $b\bar{b}$ cross section measured in the e^+e^- channel is $\Delta\sigma(b\bar{b}) = \sigma_B^A/A = 38^{+18}_{-15}$ nb/nucleon, obtained by using the weighted average of our target materials. All the parameters used in (2) are summarized in Table 2.

Different cut optimization techniques and assumptions have been tested to verify the stability of the signal. The optimizations are performed simultaneously on the three detached vertex cuts (Δz, I_w and the isolation cut) using the background from real data and the downstream $b \to J/\psi \to e^+e^-$ events from MC. Independently on the optimization criteria, a J/ψ signal with significance greater than 2 σ is always observed in the downstream part of the spectrum, while a visible J/ψ signal is never present in the upstream part. The same behavior is observed in an analysis of the electron sample performed with the muon cuts: due to less stringent vertexing requirements, both the signal and the background contributions increase, resulting however in the same final cross section value.

6 Combined cross section measurement

The two measurements, $\Delta\sigma(b\bar{b}) = 16^{+18}_{-12}$ nb/nucleon and $\Delta\sigma(b\bar{b}) = 38^{+18}_{-15}$ nb/nucleon, obtained in the muon and electron channels, respectively, are compatible within statistical uncertainties. In order to extract the maximum information on the $b\bar{b}$ production cross section from our data, we combine the $\mu^+\mu^-$ and e^+e^- likelihoods in a four parameter likelihood maximization ($\Delta\sigma(b\bar{b})$, $\mu^+\mu^-$ background slope, $\mu^+\mu^-$ and e^+e^- background yields) on the detached candidates. The fit provides our final result of the $b\bar{b}$ production cross section:

$$\Delta\sigma(b\bar{b}) = 30^{+13}_{-11}(\text{stat}) \text{ nb/nucleon}, \quad (3)$$

where the quoted uncertainty has been estimated directly from the fit (see Fig. 9).

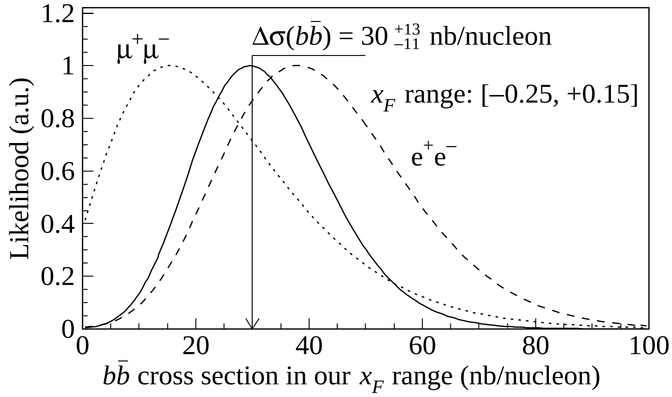

Fig. 9. The likelihood fits for the $b\bar{b}$ production cross section in our x_F range ($\Delta\sigma(b\bar{b})$) using the $\mu^+\mu^-$ and e^+e^- events separately (*dotted* and *dashed line* respectively) and in a combined analysis (*solid line*)

The main sources of systematic uncertainty in the present measurement, which are not related to the final $b\bar{b}$ statistics, are due to the prompt J/ψ cross section reference (11%), the branching ratio $\text{Br}(b\bar{b} \to J/\psi X)$ (9%), the trigger and detector simulation (5%), the prompt J/ψ MC production models (3.5%), the $b\bar{b}$ MC production models (5%), the prompt $J/\psi \to e^+e^-$ counting (5%) and the carbon-titanium difference in efficiencies (1.7%). Other contributions are below the 1% level. Uncertainties stemming from the background shapes used in the maximum likelihood fits on the invariant masses and from the cut values are dominated by the low statistics of observed detached events. For these sources we assign conservative uncertainties of $^{+10}_{-24}$% and 13% to the $\mu^+\mu^-$ and e^+e^- channels, respectively. The overall systematic uncertainty for our measurement, averaged over the muon and electron channels, is of $^{+20}_{-23}$%.

To compare our measurement with theoretical predictions, we extrapolate the $\Delta\sigma(b\bar{b})$ measurement to the full x_F range, relying on the $b\bar{b}$ production and decay model described in Sect. 3. We obtain the total $b\bar{b}$ production cross section:

$$\sigma(b\bar{b}) = 32^{+14}_{-12}(\text{stat})\,^{+6}_{-7}(\text{sys}) \text{ nb/nucleon}. \quad (4)$$

In Fig. 10, this result is compared with the latest QCD calculations [3,4] beyond next-to-leading order (NLO). The two predicted values at 920 GeV proton beam are, respectively, $\sigma(b\bar{b}) = 25^{+20}_{-13}$ nb/nucleon [2] and $\sigma(b\bar{b}) = 30 \pm 13$ nb/nucleon, in good agreement with our measurement. In the same figure, the E789 [5] and E771 [6] experimental results obtained with 800 GeV proton interactions on Au and Si, respectively, are plotted and are seen to be compatible (Fig. 10).

[2] Value based on [3], updated with the parton distribution function in [32]

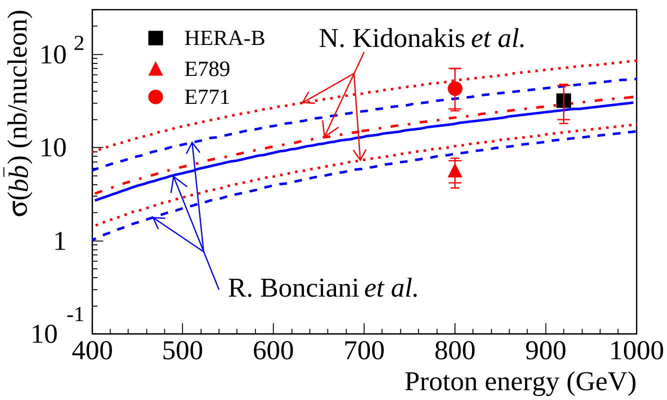

Fig. 10. The comparison of the HERA – B (2000) $\sigma(b\bar{b})$ value with other experiments and with the theoretical predictions of R. Bonciani et al. [3] updated with the NNLL parton distribution function in [32] (*solid line*: central value, *dashed lines:* upper and lower bounds) and N. Kidonakis et al. [4] (*dot-dashed line:* central value, *dotted lines:* upper and lower bounds)

7 Conclusions

Events coming from $b \to J/\psi \to l^+l^-$ decays have been identified in a sample of ≈1.35 million dilepton triggered events, acquired in a short physics run during the HERA – B commissioning period in summer 2000. The data analysis results in the identification of $1.9^{+2.2}_{-1.5}$ $b \to J/\psi \to \mu^+\mu^-$ candidates and $8.6^{+3.9}_{-3.2}$ $b \to J/\psi \to e^+e^-$ candidates.

From these candidates, we compute the $b\bar{b}$ production cross section by normalizing to the known prompt J/ψ cross section. In the J/ψ kinematic range $-0.25 < x_F < 0.15$, we obtain $\Delta\sigma(b\bar{b}) = 16^{+18}_{-12}$ nb/nucleon and $\Delta\sigma(b\bar{b}) = 38^{+18}_{-15}$ nb/nucleon in the muon and electron channels, respectively. Within statistical errors, the two results are compatible. The combined result of the $b\bar{b}$ production
cross section measured by HERA – B at 920 GeV using pC and pTi interactions in our x_F range is $\Delta\sigma(b\bar{b}) = 30^{+13}_{-11}(\text{stat}) \pm 6(\text{sys})$ nb/nucleon. Extrapolating this measurement to the full x_F range, we obtain the total $b\bar{b}$ production cross section:

$$\sigma(b\bar{b}) = 32^{+14}_{-12}(\text{stat})\,^{+6}_{-7}(\text{sys}) \text{ nb/nucleon.} \quad (5)$$

This result is compatible with the E789 [5] and E771 [6] measurements and is also in agreement with the most recent QCD predictions [3,4] beyond NLO.

Acknowledgements. We express our gratitude to the DESY laboratory and to the DESY accelerator group for their strong support since the conception of the HERA – B experiment. The HERA – B experiment would not have been possible without the enormous effort and commitment of our technical and administrative staff. It is not possible to list here the many individuals who have contributed to HERA – B. We are especially grateful to the following persons and their groups: G. Avoni, C. Baldanza, H. Bertelsen, J. Bizzell, M. Bosteels, A. Cotta-Ramusino, F. Czempik, I. D'Antone, J. Davila, J. Dicke, A. Donat, U. Dretzler, A. Epifantsev, S. Fricke, W. Funk, A. Gutierrez, F. Hansen, M. Harris, S. Hennenberger, J. Hogenbirk, M. Jablonski, V. Kiva, M. Kolander, Y. Kolotaev, L. Laptin, H. Leich, H. Lüdecke, Q. Li, K. Y. Liu, P. Liu, C. Lu, K. Ludwig, J. McGill, E. Michel, N. Murthy, E. Novikov, S. Omeltchuk, D. Padrazo, H. B. Peters, P. Pietsch, M. Pohl, N. Ratnikova, A. Rausch, W. Reinsch, P. Rose, I. Rostovtseva, R. Rusnyak, W. Sands, P. Solc, S. Starostin†, K.-H. Sulanke, V. Tchoudakov, M. Tkatch, K. Wagner, P. Wegner, V. Zerkin, E. Zimmer-Nixdorf. We thank the external HERA – B referees D. Froidevaux, R.-D. Heuer, K. Jakobs and J. Jaros for many stimulating discussions and suggestions. We are indebted to our administrative staff U. Djuanda and I. Kerkhoff for their continuous assistance. In the preparation of this paper, we have benefited from many useful discussions with M. Mangano, P. Nason, and R. Vogt on the theory of $b\bar{b}$ production.

References

1. P. Nason, QCD at High Energy, Proceedings of the XX International Symposium on Lepton and Photon Interactions at High Energies, hep-ph/0111024
2. S. Frixione et al., Adv. Ser. Direct. High Energy Phys. **15**, 609 (1998)
3. R. Bonciani et al., Nucl. Phys. B **529**, 424 (1998)
4. N. Kidonakis et al., Phys. Rev. D **64**, 114001 (2001)
5. D. M. Jansen et al., Phys. Rev. Lett. **74**, 3118 (1995)
6. T. Alexopoulos et al., Phys. Rev. Lett. **82**, 41 (1999)
7. M. H. Schub et al., Phys. Rev. D **52**, 1307 (1995)
8. T. Alexopoulos et al., Phys. Rev. D **55**, 3927 (1997)
9. D. E. Groom et al., Eur. Phys. J. C **15**, 1 (2000)
10. M. J. Leitch et al., Phys. Rev. Lett. **84**, 3256 (2000)
11. T. Alexopoulos et al., Phys. Lett. B **374**, 271 (1996)
12. M. J. Leitch et al., Phys. Rev. Lett. **72**, 2542 (1994)
13. R. Vogt, hep-ph/0111271
14. E. Hartouni et al., HERA – B Design Report, DESY-PRC-95-01 (1995)
15. The HERA – B Collaboration, HERA – B Status Report, DESY-PRC-00-04 (2000)
16. K. Ehret, Nucl. Instr. Methods A **446**, 190 (2000)
17. C. Bauer et al., Nucl. Instr. Methods A **453**, 103 (2000)
18. T. Zeuner, Nucl. Instr. Methods A **446**, 324 (2000); Y. Bagaturia et al., Nucl. Instr. Methods A **490**, 223 (2002)
19. M. Capeans, Nucl. Instr. Methods A **446**, 317 (2000)
20. J. Pyrlik, Nucl. Instr. Methods A **446**, 299 (2000); I. Ariño et al., Nucl. Instr. Methods A **453**, 289 (2000)
21. G. Avoni et al., Proc. of the IX Conference on Calorimetry in Particle Physics, Annecy, France, October 9-14, 2000, Calorimetry in High energy physics, (2001) 777; A. Zoccoli, Nucl. Instr. Methods A **446**, 246 (2000)
22. M. Buchler et al., IEEE Trans. on Nucl. Sci. **46**, 126 (1999); A. Arefiev et al., IEEE Trans. on Nucl. Sci. **48**, 1059 (2001)
23. M. Böcker et al., IEEE Trans. Nucl. Sci. **48**, 1270 (2001)
24. V. Alberico et al., Il Nuovo Cimento, **110 A**, 1453 (1997); G. Avoni et al., Nucl. Instr. Methods A **461**, 332 (2001)
25. P. Kreuzer, Nucl. Instr. Methods A **462**, 212 (2001)
26. J. M. Hernández, Proc. of the International Conference on Computing in High Energy Physics CHEP 2001, Beijing, September 2001

† *deceased*

27. J. M. Hernández, D. Ressing, V. Rybnikov, F. Sánchez, G. Wagner, Nuclear Science Symposium Conference Record, 2000 IEEE, vol.**2** (2000) 12/116
28. T. Sjöstrand, Comp. Phys. Comm. **82**, 74 (1994)
29. H. Pi, Comp. Phys. Comm. **71**, 173 (1992)
30. P. Cho, A. Leibovich, Phys. Rev. D **53**, 150 (1996)
31. M. Mangano, P. Nason, G. Ridolfi, Nucl. Phys. B **373**, 295 (1992); P. Nason, S. Dawson, R. K. Ellis, Nucl. Phys. B **327**, 49 (1988)
32. A. D. Martin, R. G. Roberts, W. J. Stirling, R. S. Thorne, Phys. Lett. B **531**, 216 (2002) hep-ph/0201127
33. J. Chay, S. D. Ellis, W. J. Stirling, Phys. Rev. D **45**, 46 (1992)
34. C. Peterson et al., Phys. Rev. D **27**, 105 (1983)
35. H. L. Lai et al., Eur. Phys. J. C **12**, 375 (2000)
36. J. Chrin, Z. Phys. **C36**, 163 (1987); D. Decamp et al., Phys. Lett. B **244**, 551 (1990); P. Nason, C. Oleari, Nucl. Phys. B **565**, 245 (2000)
37. A. Heister et al., Phys. Lett. B **512**, 30 (2001)
38. V. G. Kartvelishvili, A. K. Likhoded, V. A. Petrov, Phys. Lett. B **78**, 615 (1978)
39. R. Brun et al., GEANT3, Internal Report CERN DD/EE/84-1, CERN, 1987
40. S. Frixione *et al.*, Nucl. Phys. B **431**, 453 (1994)